Ultrafast Electron Trapping in Ligand-Exchanged Quantum Dot Assemblies

Michael E. Turk,[†] Patrick M. Vora,[†,#] Aaron T. Fafarman,[⊥,▽] Benjamin T. Diroll,[§] Christopher B. Murray,[§,‡] Cherie R. Kagan,[⊥,‡,§] and James M. Kikkawa*[,†]

[†]Department of Physics and Astronomy, [⊥]Department of Electrical and Systems Engineering, [‡]Department of Materials Science and Engineering, and [§]Department of Chemistry, University of Pennsylvania, Philadelphia, Pennsylvania 19104, United States. [#]Present address: School of Physics, Astronomy, and Computational Sciences, George Mason University, Fairfax, Virginia 22030, United States. [▽]Present address: Chemical & Biological Engineering Department, Drexel University, Philadelphia, Pennsylvania 19104, United States.

ABSTRACT We use time-integrated and time-resolved photoluminescence and absorption to characterize the low-temperature optical properties of CdSe quantum dot solids after exchanging native aliphatic ligands for thiocyanate and subsequent thermal annealing. In contrast to trends established at room temperature, our data show that at low temperature the band-edge absorptive bleach is dominated by $1S_{3/2h}$ hole occupation in the quantum dot interior. We find that our ligand treatments, which bring enhanced interparticle coupling, lead to faster surface state electron trapping, a greater proportion of surface-related photoluminescence, and decreased band-edge photoluminescence lifetimes.

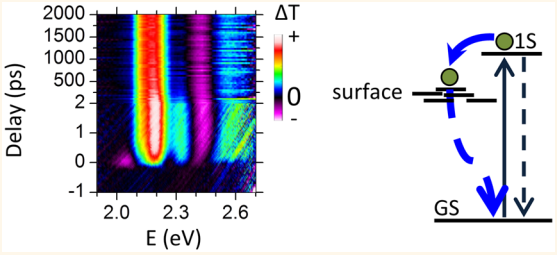

KEYWORDS: cadmium selenide · quantum dots · ligand exchange · time-resolved absorption · ultrafast fluorescence · electron trapping

Semiconductor quantum dots (QDs) have been the focus of intense study for their size-tunable properties with applications in light-emitting devices, photovoltaic devices, and printable electronics.[1−6] The size, shape, composition, and surface chemistry of QDs, as well as their temperature and local environment, are all of great importance, modifying photoluminescence (PL) yields, shifting optical transitions, and impacting electrical conductivity.[7−18] Time-resolved optical spectroscopies can directly monitor relaxation pathways that respond sensitively to these parameters, and there exists a rich literature measuring the population-averaged response of QDs dispersed in solutions and polymer matrices.[19−24] To date, ultrafast optical studies of close-packed colloidal QD solids have been more limited in number,[15,25−29] and although the majority of these studies have typically been performed at room temperature, measurements at low temperature offer the potential for increased sensitivity to environmental changes as well as a sharper view of relaxation processes.

In this report, we study the impact of surface treatment on the low temperature (10 K) optical properties of CdSe QD solids. The ligand exchange and annealing process used here[13] has laid the foundation for high mobility CdSe field effect transitors, where the role of surface traps is underscored by the need to use indium to passivate the QD surfaces and to increase the Fermi energy in order to reduce a mobility gap.[16,30] Here we employ time-resolved absorption (TRA) and photoluminescence (TRPL) spectroscopies to gain insight into the ligand exchange and annealing process through excited state dynamics. Because both TRA and TRPL implementations developed here are broadband with subpicosecond time resolution, we are able to show that exchanging aliphatic native ligands (NL) for thiocyanate (SCN) and subsequently annealing the samples increases electron trapping rates by 2 orders of magnitude. We demonstrate a need to modify the conventional interpretation of CdSe QD time-resolved absorption spectra in this experimental configuration and show that the electron, not the hole, traps first out of the core excitonic state.

RESULTS AND DISCUSSION

Time-*integrated* optical absorption spectroscopy is routinely used for the characterization

* Address correspondence to kikkawa@physics.upenn.edu.

Received for review October 14, 2014 and accepted January 30, 2015.

Published online January 30, 2015
10.1021/nn505862g

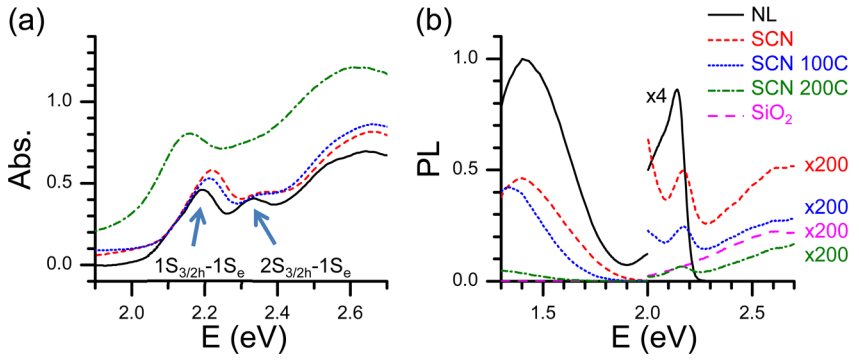

Figure 1. (a) Optical absorption and (b) photoluminescence spectra excited at 3.1 eV at 10 K for CdSe QD solids and a fused silica (SiO_2) substrate. CdSe QD solids passivated with NL (black, solid line), SCN (red, dashed line), SCN annealed at 100 °C (blue dot), SCN annealed at 200 °C (green dash dot), and fused silica (b only, purple long dash). Arrows (a) mark optical transitions.

of QD systems, providing information on sample size and homogeneity, as well as interparticle coupling.[31−33] As previously reported for similar samples, SCN ligand substitution and thermal annealing shifts and broadens the quantized band-edge optical absorption peak ($1S_{3/2h}1S_e$ in the effective mass approximation[34]) in these QD solids (Figure 1a, room temperature in Supporting Information Figure S1).[13] Whereas time-integrated absorption reflects the optical properties of core states,[35] time-integrated band-edge PL is heavily impacted by conditions that influence carrier trapping to the surface.[7,36] We study four samples: CdSe QD solids with native, aliphatic ligands (NL); native ligands exchanged for SCN (SCN); exchanged and subsequently annealed at 100 °C (SCN 100C); and exchanged and subsequently annealed at 200 °C (SCN 200C). As previously shown by several of us using scanning electron, atomic force, and optical microscopies on identically prepared samples (see ref 16 and Supporting Information Figure S2a,b), the sample preparation and spin-coating process used here and described below produces uniform, randomly close-packed, optically smooth, and crack-free thin films over large areas. Fourier transform infrared spectroscopy (FTIR) shows that SCN exchanges 90% of the NL ligands used in synthesis, and that annealing to 200 °C significantly decomposes SCN (see ref 16 and Supporting Information Figure S2c).

The exchange and annealing processes dramatically decrease both the total integrated PL (band-edge plus sub-bandgap, surface emission) and the relative strength of band-edge PL compared to surface emission (Figure 1b and Supporting Information Figure S3). While band-edge PL requires both an electron and a hole in a QD core state,[37] sub-bandgap PL involves QD surface states for which carrier hops back to higher energy core states require thermal fluctuations that are unlikely at 10 K.[8,12,38−40] Band-edge photoluminescence is therefore unlikely after any carriers have trapped to surface states, and the decreased band-edge PL relative to surface emission after exchange and annealing is a signature of an increased surface trapping rate in these samples.

Time-resolved photoluminescence (TRPL) measurements can provide more direct insight into the non-equilibrium kinetics of QDs and help to clarify the interplay of core and surface states.[12,39,41−46] Previous TRPL studies have demonstrated long radiative lifetimes from surface trapped states, attributing these trap states to electron traps at unpassivated Cd or hole traps at unpassivated Se.[12,39,40] Annealing to 100 °C is not expected to change the QD surface properties significantly, whereas annealing to 200 °C decomposes SCN and we may then expect a concomitant change in charge dynamics.[16]

TRPL measurements, shown in Figure 2, reveal dramatic decreases in band-edge PL lifetime with ligand exchange and annealing, showing that changes in time-integrated PL reflect dynamical changes upon QD surface treatment. The PL signal from the pristine NL sample decays over hundreds of picoseconds in agreement with previous short-time TRPL measurements,[45] but the exchange of NL for SCN drastically shortens the PL lifetime to tens of picoseconds. Annealing the exchanged sample at 100 °C leaves TRPL decays largely unchanged, but further annealing to 200 °C hastens the TRPL decay so the observed transient approaches the instrument response limit. The decreases in TRPL lifetime in exchanged and annealed samples echo decreases in time-integrated band-edge PL (Figure 1 and Supporting Information Figure S3a), and indicate increased capture rates of the bright exciton by pathways other than band-edge PL. The latter may include nonradiative relaxation, although the increase in relative quantum yield for surface state emission (Supporting Information Figure S3b) indicates that some portion emerges as surface PL.

Our PL data, taken by itself, could be rationalized in terms of our surface treatments. In particular, decay pathways alternative to band-edge PL could arise from a higher trap density upon exchange, which is further increased upon annealing at 200 °C. The replacement

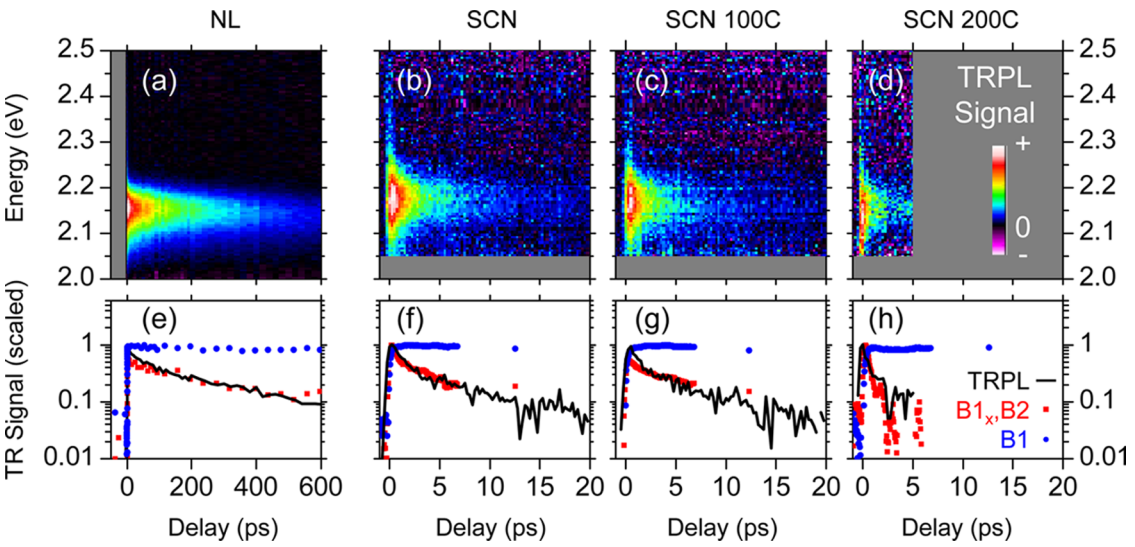

Figure 2. (a–d) Time-resolved photoluminescence spectral maps at 10 K for CdSe QD thin films with (a) NL, (b) SCN, (c) SCN annealed at 100 °C, and (d) SCN annealed at 200 °C. (e–h) Spectrally integrated TRPL (black) compared and contrasted with TRA features {B1$_x$, B2} (red) and B1 (blue). Note that panels a and e show different time scales than the other panels (b–d, f–h). TRPL maps are scaled for contrast.

of NL by SCN (without annealing) increases the number of electron and hole traps on unpassivated surface atoms due to reduced overall surface coverage,[13,47] and is expected to further introduce hole traps associated with the SCN ligands,[40,47] so the appearance of additional traps after exchange is easily understood.[48] Moreover, thermal annealing to 200 °C decomposes SCN and leaves S atoms bonded to Cd (see refs 16, 49, and Supporting Information Figure S2c), a process likewise expected to increase the number of hole traps in the SCN 200C sample.[17] Although these increases in hole trap density could account for the progressive decrease in PL lifetimes, considerations of TRA described below indicate an increase in *electron* trapping.

Time-resolved absorption (TRA) measures pump-induced changes in transmission, $\Delta T/T_0$, subsequent to pump excitation. Quantum dot TRA measurements have a long history in measuring carrier relaxation and the impact of surface treatments, and signals emerge from numerous effects including bleached transitions from state-filling, shifts in absorption spectra leading to photoinduced absorptions, exciton–phonon coupling that modulates TRA signals, and optical gain.[7,21,50–54] Prior TRA experiments have shown that electrons relax quickly to the band edge through Auger heating of the holes[19] and ligand interactions[55] and that holes relax primarily through ligand interactions with minor contributions from phonons.[56] Figure 3a superimposes a time-integrated absorption spectrum (black), a scaled exemplary TRA time slice (red), and a corresponding TRA 2D map. Features A1, B1, and B2 are labeled following the convention introduced in ref 57. Figure 3b shows schematically the corresponding single particle electron and hole states associated with these transitions.[34] The energetic location and time duration

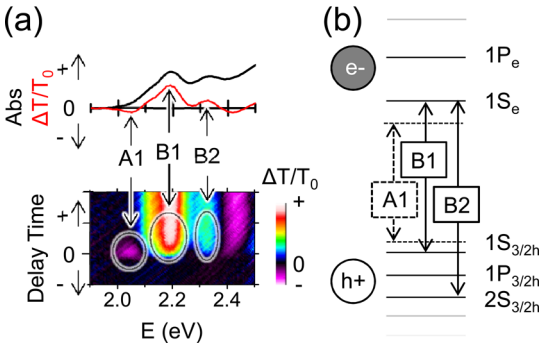

Figure 3. (a) Scaled time-integrated absorption spectrum (black) and time-resolved absorption spectrum (red, 0–0.5 ps) for CdSe NL QD thin film sample showing photoinduced absorption feature A1 and bleach features B1 and B2. (b) Correspondence between time-resolved absorption features and QD optical transitions as described in text.

of the photoinduced absorption A1 probe the biexciton binding energy and hot-exciton relaxation,[20,51] and the presence of the bleach signals labeled B1 and B2 indicate decreased transition strength at the $1S_{3/2h}1S_e$ and $2S_{3/2h}1S_e$ optical transitions, respectively.[57] Because the physical interpretation of time-resolved absorption signals at energies above the B2 feature is complicated by the high density of optical transitions, we do not focus on interpreting those features in this report.[34]

These optical transitions can in principle be bleached by the presence of charge carriers in either or both of the constituent hole or electron states of the QD. We will label the subcomponents of the B1 bleach as $B1_x$, $B1_e$, and $B1_h$, for which absorption at the $1S_{3/2h}1S_e$ transition is blocked by occupancy of the $1S_{3/2h}1S_e$ exciton, electron, and $1S_{3/2h}$ hole states of the QD, respectively. Within the band-edge B1 bleach

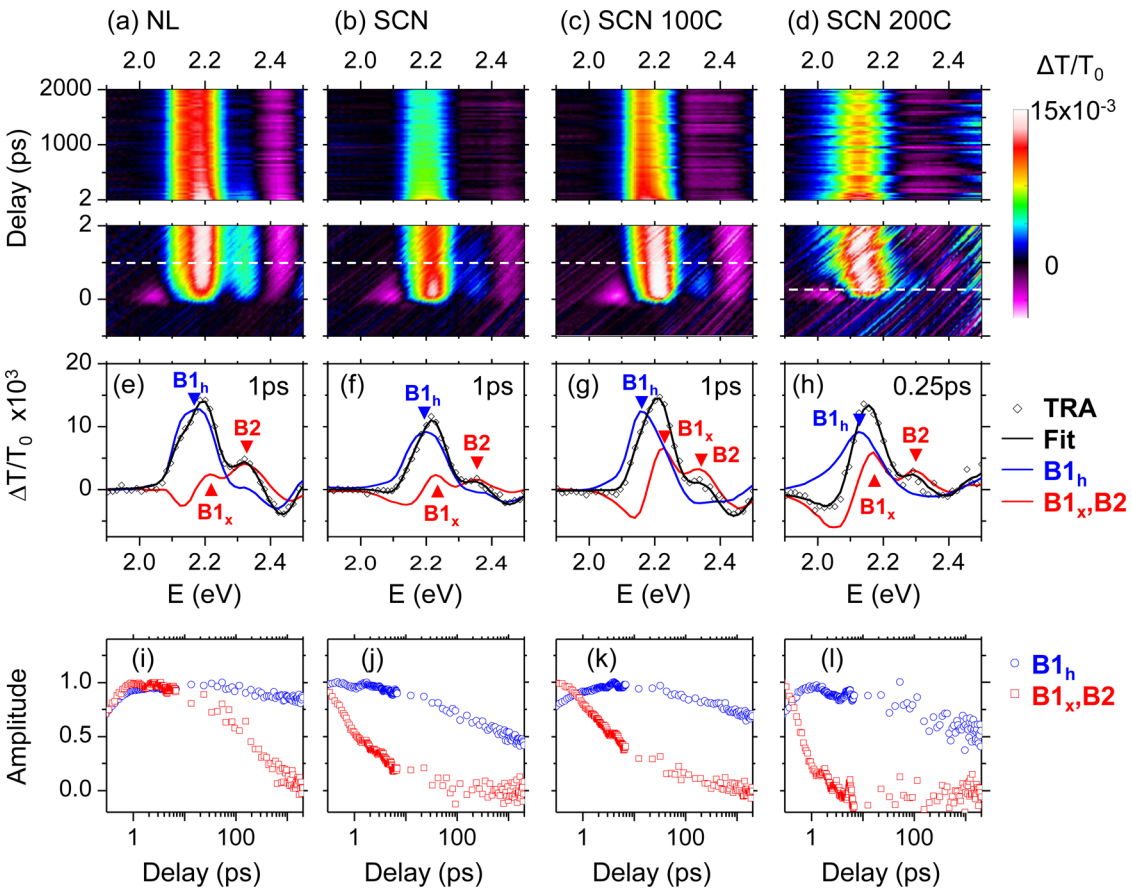

Figure 4. Time-resolved absorption (a–d) spectral maps, (e–h) time slices, and (i–l) decay profiles at 10 K for CdSe QD thin films. Dotted lines in spectral maps indicate the times for which time slices are taken. Samples are (a,e,i) NL, (b,f,j) SCN, (c,g,k) SCN annealed at 100 °C, and (d,h,l) SCN annealed at 200 °C. TRA maps are fit using two principal spectra (blue and red lines in e–h) and their decay profiles (blue and red symbols in i–l). Spectral maps are negative-time background subtracted.

the precise location of $B1_x$, $B1_e$, and $B1_h$ vary to some extent,[58,59] but this variation is much less than the separation between the B1 and B2 bands.

The TRA 2D maps in Figure 4a–d show that the aggregate B1 bleach in all samples persists beyond the 2 ns time window of this experiment and significantly beyond the subnanosecond decay of TRPL observed in all samples. This difference can be quickly seen by comparing TRA B1 (blue) and TRPL (black) curves in Figure 2e–h. Thus, the dynamics of B1 are relatively insensitive to surface treatment when compared to TRPL. Because the TRPL decay measures the depopulation of core *excitons*, the presence of B1 well after band-edge TRPL disappears must be due to only $B1_e$ or $B1_h$, or conversion to a dark[60] exciton. Because of the relative similarity of B1 dynamics among the samples and the progressively faster decay of TRPL upon exchange and annealing, we may conclude that the surface treatment process used here predominantly modifies the decay kinetics of only one charge carrier, or accelerates interconversion to the dark exciton.

Further inspection of Figure 4a–d indicates that these surface treatments hasten *electron* surface trapping. First, the rapid decay of the A1 absorption feature (circled in Figure 3a) shows that excitons relax to the $1S_{3/2h}1S_e$ state within the first picosecond,[20] and since $kT \approx 1$ meV is much smaller than the 100 meV separation of the $1S_{3/2h}$ and $2S_{3/2h}$ states, Boltzmann occupation of the $2S_{3/2h}$ states is minimal. Subsequent dynamics of the B2 bleach therefore cannot reflect $2S_{3/2h}$ hole state occupation and must arise from the $1S_e$ electron. Second, the dramatic changes in decay rate for B2 upon surface treatment are closely matched by similar changes in the TRPL (red and black curves in Figure 2e–h, respectively). We may therefore identify electron surface trapping as the process that gives rise to rapid PL quenching and decreases the time-integrated photoluminescence yield in the SCN, SCN 100C, and SCN 200C samples. Note that because transitions to both the $1S_{3/2h}1S_e$ and $2S_{3/2h}1S_e$ exciton states require available $1S_e$ states,[34] an electron in the $1S_e$ state should contribute bleaches to both B1 and B2.[50] At room temperature it has been commonly observed that the decays of B1 and B2 mirror each other, implicating occupation of the $1S_e$ state as a common denominator.[19,20,61] In contrast, in our low-temperature measurements the lifetime of the aggregate B1 bleach is much longer than that of B2 for all samples (Figure 4a–d and Figure 2e–h), which cannot be due to a $1S_e$ electron or a dark exciton. We instead attribute the longer life of

B1 relative to B2 to the presence of a long-lived hole in the $1S_{3/2h}$ state and interpret the decay of the B2 bleach as reflecting the rapid surface trapping of an electron that leaves this hole remaining in the QD core.

The hole contribution to B1 is commonly argued to be small in principle due to greater degeneracy of the hole states and thermal distribution of holes to higher-lying states.[50] To assess the plausibility that the $B1_h$ bleach due to hole state occupation can contribute significantly to the B1 transition at low temperatures, we consider the impact of thermal state occupation on available optical transitions in relevant electron−hole charge configurations. Previous calculations by Califano, *et al.*, showed that excitons, biexcitons, and trions have different radiative lifetimes.[58] In the Supporting Information we use these predictions to calculate expected B1 TRA amplitudes from each charge configuration using a Boltzmann distribution of initial state occupations for electrons, holes, and excitons. In contrast to prior assertions that B1 measures only the $1S_e$ occupation in CdSe QDs (in our framework either through $B1_x$ or $B1_e$),[19,20,61] our calculations indicate that the presence of *either* an electron or a hole in the QD core produces a strong B1 TRA signal at all temperatures from 10 to 300 K with only a weak temperature dependence. Although predictions show the contribution of an exciton to B1 is greater than that of a hole or an electron, the predicted $B1_h$ signal from the hole is actually stronger than the $B1_e$ signal due to the electron at all temperatures calculated. These calculations confirm that a core-state hole can efficiently bleach the B1 transition at 10 K, validating our assignment of the long-lived B1 signal to $B1_h$.

Analysis of the fine structure within B1 further reinforces these conclusions. Figure 4a−d show that the aggregate B1 feature redshifts with time in all samples, and the TRA spectra, particularly Figure 4e−g, show that this redshift actually corresponds to a redistribution of amplitude between two peaks within B1. We denote the lower (higher) energy peak $B1_h$ ($B1_x$), nomenclature validated by their temporal dynamics. Analysis using singular value decomposition, described in the Supporting Information, identifies two distinct temporal behaviors that account for the TRA maps for all but subpicosecond time delays. A long-lived component is associated with the lower energy peak $B1_h$, and a short-lived contribution is associated with the upper energy peak $B1_x$ *as well as B2*. The spectra and time dependence of the long- and short-lived components are shown in Figures 4e−h and 4i−l, respectively. A third, subpicosecond component described in the Supporting Information is associated with thermalization of hot carriers. These findings reveal that the temporal dynamics of B2 not only mirror the dynamics of TRPL, but also $B1_x$ (Figure 2e−h). Since B2 measures electron occupation, the accord between B2 and $B1_x$ indicates that the decay of $B1_x$ reflects the destruction of the $1S_{3/2h}1S_e$ exciton through electron trapping to the surface. Additionally, the agreement between $B1_x$ and TRPL indicates that $B1_x$ measures the population of *bright* excitons. In Figure 4i−l we summarize the temporal evolution of $B1_h$, $B1_x$, and B2, whose associated peaks are marked by triangles in Figure 4e−h. Since we have already established that the B1 component that out-lasts both TRPL and B2 is due to $1S_{3/2h}$ holes in the QD core, the remaining lower energy component of B1 is $B1_h$. We note that in this analysis $B1_x$ and $B1_h$ are separated by more than 30 meV in all four samples. Although relaxation of an exciton from the lowest energy bright exciton state into the optically forbidden dark state[60,62] would redshift the B1 feature,[63] as discussed above the trapped electron evidenced by the B2 decay precludes this as an explanation for $B1_h$.

Given the expectation discussed earlier that exchange and annealing principally increase the density of hole traps, our finding that these treatments primarily increase electron trapping is surprising. One mitigating consideration is that, to the extent that Cd−S surface bonds may be viewed as assembling a CdS shell, hole trapping may be impeded by differences in bandgap and by the formation of a quasi-type-II band alignment, which further localizes the hole in samples sufficiently annealed to decompose SCN.[64,65] We also note that cyclic voltammetry measurements of samples annealed at 250 °C have shown that such annealing introduces midgap states close to both the conduction and valence band edges, and that the former may introduce electron traps in the SCN 200C sample.[47]

Additionally, increased coupling between QDs may introduce trapping pathways that do not arise in isolated QDs. For example, the increased interparticle coupling and greater electrical conductivity previously demonstrated in these SCN exchanged samples[13] likely increase exciton and charge carrier diffusion to lower energy QDs.[27] Recent room temperature studies of QD solids demonstrated that excitons can become concentrated at low energy "hotspots", enabling multiexciton phenomena when excitation densities surpass a rather low threshold of 10^{-3} excitons per quantum dot.[66] Under these conditions, which are met in this study, Auger processes can produce fast, radiationless recombination as well as hot carrier generation that enhances the likelihood of carrier trapping. Electron trapping would benefit more from the latter because kinetic relaxation is more facile for holes. Greater coupling, combined with spatial disorder in the degree of that coupling, can also explain the fast blueshift in TRPL observed in the SCN 200C sample (Figure 2d). By the arguments given above, PL transients from more highly coupled regions would decay more quickly. Since those regions would tend to have lower energy band-edge emission,[13] once this contribution decays the remaining TRPL signal would shift to higher energies as observed.

CONCLUSION

Low temperature time-resolved optical measurements of these QD solids show progressively faster electron trapping to the QD surface upon ligand exchange and annealing. Combining time-resolved absorption and photoluminescence, we find that holes within the QD, rather than electrons, are responsible for the bleach of the band-edge transition. Our finding that electron trapping is dominant at low temperature comes as a surprise given what is known about the surface treatment in these QDs. Although we argue that enhanced interparticle electronic coupling may increase electron trapping through multiexciton phenomena, additional study is needed to understand the interplay between electron and hole traps in this system.

METHODS

Cadmium selenide QDs passivated with aliphatic ligands are prepared by the method described by Qu and Peng and processed as previously described by Fafarman *et al.*[13,67] The native ligands are solution exchanged with SCN, and samples are then spin-cast onto 0.5 mm thick UV fused silica substrates (MTI Corporation) prescored on the back surface for cleaving and, wherever indicated, annealed under nitrogen on a hot plate for 5 min to increase electronic coupling among QDs. Extensive characterization of films resulting from this process is reported in ref 16. Sample substrates are cleaved and mounted in an optical cryostat (Oxford Microstat-HE) under a majority argon atmosphere that is immediately evacuated.

TRPL is performed with a home-built apparatus partially described previously[68,69] that permits broadband study of short delay times without determining *a priori* the wavelength range of interest. An experimental schematic and description is provided in the Supporting Information, which shows the updated configuration that allows measurement of TRA as well (Supporting Information Figure S5). Briefly, TRPL and TRA are excited using the 400 nm doubled output of a 1 kHz, 120 fs regenerative amplifier. For TRPL, the 800 nm fundamental beam is used to create an optical Kerr gate (OKG).[70,71] For TRA, the fundamental beam is sampled to generate a white light supercontinuum. The chirp of the white light supercontinuum probe is calibrated with the OKG (Supporting Information Figure S6). Instrument response times for the TRPL and TRA experiments are approximately 500 and 120 fs as configured. Spectral resolution as configured is 10 nm for absorption measurements and 13 nm for photoluminescence measurements. Less than 0.1 photons are absorbed per QD per pulse.[35,72] Further experimental details appear in the Supporting Information.

Singular value decomposition analysis of TRA spectra is described in the Supporting Information. This analysis yields the temporal decays of $B1_h$, $B1_x$, and B2 shown in Figures 2 and 4. The aggregate B1 bleach signal, denoted simply "B1", is computed by integrating the B1 bleach over its bandwidth (1.9 to 2.3 eV).

Conflict of Interest: The authors declare no competing financial interest.

Acknowledgment. All aspects of this work are supported by the U.S. Department of Energy Office of Basic Energy Sciences, Division of Materials Science and Engineering, under Award No. DE-SC0002158.

Supporting Information Available: Room temperature optical absorption spectra, atomic force microscopy, FTIR spectra, photoluminescence intensity comparisons, calculations of relative contributions of electrons and holes to TRA spectra, experimental apparatus description and schematic, chirp correction method, TRPL background reduction technique, discussion of TRA reproducibility, and details of SVD analysis. This material is available free of charge *via* the Internet at http://pubs.acs.org.

REFERENCES AND NOTES

1. Kramer, I. J.; Sargent, E. H. The Architecture of Colloidal Quantum Dot Solar Cells: Materials to Devices. *Chem. Rev.* **2014**, *114*, 863–882.
2. Kim, J. Y.; Voznyy, O.; Zhitomirsky, D.; Sargent, E. H. 25th Anniversary Article: Colloidal Quantum Dot Materials and Devices: A Quarter-Century of Advances. *Adv. Mater.* **2013**, *25*, 4986–5010.
3. Hetsch, F.; Zhao, N.; Kershaw, S. V.; Rogach, A. L. Quantum Dot Field Effect Transistors. *Mater. Today* **2013**, *16*, 312–325.
4. Shirasaki, Y.; Supran, G. J.; Bawendi, M. G.; Bulovic, V. Emergence of Colloidal Quantum-Dot Light-Emitting Technologies. *Nat. Photonics* **2013**, *7*, 13–23.
5. Kim, T.-H.; Cho, K.-S.; Lee, E. K.; Lee, S. J.; Chae, J.; Kim, J. W.; Kim, D. H.; Kwon, J.-Y.; Amaratunga, G.; Lee, S. Y.; *et al.* Full-Colour Quantum Dot Displays Fabricated by Transfer Printing. *Nat. Photonics* **2011**, *5*, 176–182.
6. Kim, D. K.; Lai, Y.; Diroll, B. T.; Murray, C. B.; Kagan, C. R. Flexible and Low-Voltage Integrated Circuits Constructed from High-Performance Nanocrystal Transistors. *Nat. Commun.* **2012**, *3*, 1216.
7. Peterson, M. D.; Cass, L. C.; Harris, R. D.; Edme, K.; Sung, K.; Weiss, E. A. The Role of Ligands in Determining the Exciton Relaxation Dynamics in Semiconductor Quantum Dots. *Annu. Rev. Phys. Chem.* **2014**, *65*, 317–339.
8. Mooney, J.; Krause, M. M.; Saari, J. I.; Kambhampati, P. A Microscopic Picture of Surface Charge Trapping in Semiconductor Nanocrystals. *J. Chem. Phys.* **2013**, *138*, 204705.
9. Hines, D. A.; Kamat, P. V. Recent Advances in Quantum Dot Surface Chemistry. *ACS Appl. Mater. Interfaces* **2014**, *6*, 3041–3057.
10. Kagan, C.; Murray, C.; Nirmal, M.; Bawendi, M. Electronic Energy Transfer in CdSe Quantum Dot Solids. *Phys. Rev. Lett.* **1996**, *76*, 1517–1520.
11. Mooney, J.; Krause, M. M.; Kambhampati, P. Connecting the Dots: The Kinetics and Thermodynamics of Hot, Cold, and Surface-Trapped Excitons in Semiconductor Nanocrystals. *J. Phys. Chem. C* **2014**, *118*, 7730–7739.
12. Baker, D. R.; Kamat, P. V. Tuning the Emission of CdSe Quantum Dots by Controlled Trap Enhancement. *Langmuir* **2010**, *26*, 11272–11276.
13. Fafarman, A. T.; Koh, W.-k.; Diroll, B. T.; Kim, D. K.; Ko, D.-K.; Oh, S. J.; Ye, X.; Doan-Nguyen, V.; Crump, M. R.; Reifsnyder, D. C.; et al. Thiocyanate-Capped Nanocrystal Colloids: Vibrational Reporter of Surface Chemistry and Solution-Based Route to Enhanced Coupling in Nanocrystal Solids. *J. Am. Chem. Soc.* **2011**, *133*, 15753–15761.
14. Chung, D. S.; Lee, J.-S.; Huang, J.; Nag, A.; Ithurria, S.; Talapin, D. V. Low Voltage, Hysteresis Free, and High Mobility Transistors from All-Inorganic Colloidal Nanocrystals. *Nano Lett.* **2012**, *12*, 1813–1820.
15. Crisp, R. W.; Schrauben, J. N.; Beard, M. C.; Luther, J. M.; Johnson, J. C. Coherent Exciton Delocalization in Strongly Coupled Quantum Dot Arrays. *Nano Lett.* **2013**, *13*, 4862–4869.
16. Choi, J.-H.; Fafarman, A. T.; Oh, S. J.; Ko, D.-K.; Kim, D. K.; Diroll, B. T.; Muramoto, S.; Gillen, J. G.; Murray, C. B.; Kagan, C. R. Bandlike Transport in Strongly Coupled and Doped Quantum Dot Solids: A Route to High-Performance Thin-Film Electronics. *Nano Lett.* **2012**, *12*, 2631–2638.
17. Kim, D. K.; Fafarman, A. T.; Diroll, B. T.; Chan, S. H.; Gordon, T. R.; Murray, C. B.; Kagan, C. R. Solution-Based

Stoichiometric Control over Charge Transport in Nanocrystalline CdSe Devices. *ACS Nano* **2013**, *7*, 8760–8770.
18. Lee, J.-S.; Kovalenko, M. V.; Huang, J.; Chung, D. S.; Talapin, D. V. Band-Like Transport, High Electron Mobility and High Photoconductivity in All-Inorganic Nanocrystal Arrays. *Nat. Nanotechnol.* **2011**, *6*, 348–352.
19. Klimov, V. I.; McBranch, D. W.; Leatherdale, C. A.; Bawendi, M. G. Electron and Hole Relaxation Pathways in Semiconductor Quantum Dots. *Phys. Rev. B* **1999**, *60*, 13740–13749.
20. Sewall, S.; Cooney, R.; Anderson, K.; Dias, E.; Kambhampati, P. State-to-State Exciton Dynamics in Semiconductor Quantum Dots. *Phys. Rev. B* **2006**, *74*, 235328.
21. Kambhampati, P. Hot Exciton Relaxation Dynamics in Semiconductor Quantum Dots: Radiationless Transitions on the Nanoscale. *J. Phys. Chem. C* **2011**, *115*, 22089–22109.
22. Chuang, C.-H.; Chen, X.; Burda, C. Femtosecond Time-Resolved Hot Carrier Energy Distributions of Photoexcited Semiconductor Quantum Dots. *Ann. Phys.* **2013**, *525*, 43–48.
23. Griffin, G. B.; Ithurria, S.; Dolzhnikov, D. S.; Linkin, A.; Talapin, D. V.; Engel, G. S. Two-Dimensional Electronic Spectroscopy of CdSe Nanoparticles at Very Low Pulse Power. *J. Chem. Phys.* **2013**, *138*, 014705.
24. Knowles, K. E.; McArthur, E. A.; Weiss, E. A. A Multi-Timescale Map of Radiative and Nonradiative Decay Pathways for Excitons in CdSe Quantum Dots. *ACS Nano* **2011**, *5*, 2026–2035.
25. Tvrdy, K.; Kamat, P. V. Substrate Driven Photochemistry of CdSe Quantum Dot Films: Charge Injection and Irreversible Transformations on Oxide Surfaces. *J. Phys. Chem. A* **2009**, *113*, 3765–3772.
26. Kraabel, B.; Malko, A.; Hollingsworth, J.; Klimov, V. I. Ultrafast Dynamic Holography in Nanocrystal Solids. *Appl. Phys. Lett.* **2001**, *78*, 1814–1816.
27. Gao, Y.; Talgorn, E.; Aerts, M.; Trinh, M. T.; Schins, J. M.; Houtepen, A. J.; Siebbeles, L. D. A. Enhanced Hot-Carrier Cooling and Ultrafast Spectral Diffusion in Strongly Coupled PbSe Quantum-Dot Solids. *Nano Lett.* **2011**, *11*, 5471–5476.
28. Boehme, S. C.; Walvis, T. A.; Infante, I.; Grozema, F. C.; Vanmaekelbergh, D.; Siebbeles, L. D. A.; Houtepen, A. J. Electrochemical Control over Photoinduced Electron Transfer and Trapping in CdSe-CdTe Quantum-Dot Solids. *ACS Nano* **2014**, *8*, 7067–7077.
29. Talgorn, E.; Gao, Y.; Aerts, M.; Kunneman, L. T.; Schins, J. M.; Savenije, T. J.; van Huis, M. A.; van der Zant, H. S. J.; Houtepen, A. J.; Siebbeles, L. D. A. Unity Quantum Yield of Photogenerated Charges and Band-Like Transport in Quantum-Dot Solids. *Nat. Nanotechnol.* **2011**, *6*, 733–739.
30. Turk, M. E.; Choi, J.-H.; Oh, S. J.; Fafarman, A. T.; Diroll, B. T.; Murray, C. B.; Kagan, C. R.; Kikkawa, J. M. Gate-Induced Carrier Delocalization in Quantum Dot Field Effect Transistors. *Nano Lett.* **2014**, *14*, 5948–5952.
31. Yu, W.; Qu, L.; Guo, W.; Peng, X. Experimental Determination of the Extinction Coefficient of CdTe, CdSe, and CdS Nanocrystals. *Chem. Mater.* **2003**, *15*, 2854–2860.
32. Foos, E. E. The Complex Interaction of Spectroscopic Shifts and Electronic Properties in Semiconductor Nanocrystal Films. *J. Phys. Chem. Lett.* **2013**, *4*, 625–632.
33. Leatherdale, C. A.; Bawendi, M. G. Observation of Solvatochromism in CdSe Colloidal Quantum Dots. *Phys. Rev. B* **2001**, *63*, 165315.
34. Norris, D. J.; Bawendi, M. G. Measurement and Assignment of the Size-Dependent Optical Spectrum in CdSe Quantum Dots. *Phys. Rev. B* **1996**, *53*, 16338–16346.
35. Leatherdale, C.; Woo, W.-K.; Mikulec, F.; Bawendi, M. On the Absorption Cross Section of CdSe Nanocrystal Quantum Dots. *J. Phys. Chem. B* **2002**, *106*, 7619–7622.
36. Kalyuzhny, G.; Murray, R. Ligand Effects on Optical Properties of CdSe Nanocrystals. *J. Phys. Chem. B* **2005**, *109*, 7012–7021.
37. Kuno, M.; Lee, J. K.; Dabbousi, B. O.; Mikulec, F. V.; Bawendi, M. G. The Band Edge Luminescence of Surface Modified CdSe Nanocrystallites: Probing the Luminescing State. *J. Chem. Phys.* **1997**, *106*, 9869–9882.
38. Mooney, J.; Krause, M. M.; Saari, J. I.; Kambhampati, P. Challenge to the Deep-Trap Model of the Surface in Semiconductor Nanocrystals. *Phys. Rev. B* **2013**, *87*, 081201.
39. Underwood, D.; Kippeny, T.; Rosenthal, S. Ultrafast Carrier Dynamics in CdSe Nanocrystals Determined by Femtosecond Fluorescence Upconversion Spectroscopy. *J. Phys. Chem. B* **2001**, *105*, 436–443.
40. Buckley, J. J.; Couderc, E.; Greaney, M. J.; Munteanu, J.; Riche, C. T.; Bradforth, S. E.; Brutchey, R. L. Chalcogenol Ligand Toolbox for CdSe Nanocrystals and Their Influence on Exciton Relaxation Pathways. *ACS Nano* **2014**, *8*, 2512–2521.
41. Jones, M.; Lo, S. S.; Scholes, G. D. Quantitative Modeling of the Role of Surface Traps in CdSe/CdS/ZnS Nanocrystal Photoluminescence Decay Dynamics. *Proc. Natl. Acad. Sci. U.S.A.* **2009**, *106*, 3011–3016.
42. Jones, M.; Scholes, G. D. On the Use of Time-Resolved Photoluminescence as a Probe of Nanocrystal Photoexcitation Dynamics. *J. Mater. Chem.* **2010**, *20*, 3533–3538.
43. Garrett, M. D.; Dukes, A. D., III; McBride, J. R.; Smith, N. J.; Pennycook, S. J.; Rosenthal, S. J. Band Edge Recombination in CdSe, CdS and CdS_xSe_{1-x} Alloy Nanocrystals Observed by Ultrafast Fluorescence Upconversion: The Effect of Surface Trap States. *J. Phys. Chem. C* **2008**, *112*, 12736–12746.
44. Wuister, S. F.; de Mello Donega, C.; Meijerink, A. Influence of Thiol Capping on the Exciton Luminescence and Decay Kinetics of CdTe and CdSe Quantum Dots. *J. Phys. Chem. B* **2004**, *108*, 17393–17397.
45. Morello, G.; Anni, M.; Cozzoli, P.; Manna, L.; Cingolani, R.; De Giorgi, M. Picosecond Photoluminescence Decay Time in Colloidal Nanocrystals: The Role of Intrinsic and Surface States. *J. Phys. Chem. C* **2007**, *111*, 10541–10545.
46. Jones, M.; Lo, S. S.; Scholes, G. D. Signatures of Exciton Dynamics and Carrier Trapping in the Time-Resolved Photoluminescence of Colloidal CdSe Nanocrystals. *J. Phys. Chem. C* **2009**, *113*, 18632–18642.
47. Choi, J.-H.; Oh, S. J.; Lai, Y.; Kim, D. K.; Zhao, T.; Fafarman, A. T.; Diroll, B. T.; Murray, C. B.; Kagan, C. R. *In Situ* Repair of High-Performance, Flexible Nanocrystal Electronics for Large-Area Fabrication and Operation in Air. *ACS Nano* **2013**, *7*, 8275–8283.
48. Jasieniak, J.; Mulvaney, P. From Cd-Rich to Se-Rich—The Manipulation of CdSe Nanocrystal Surface Stoichiometry. *J. Am. Chem. Soc.* **2007**, *129*, 2841–2848.
49. Gunasekaran, S.; Ponnusamy, S. Growth and Characterization of Cadmium Magnesium Tetra Thiocyanate Crystals. *Cryst. Res. Technol.* **2006**, *41*, 130–137.
50. Klimov, V. I. Spectral and Dynamical Properties of Multiexcitons in Semiconductor Nanocrystals. *Annu. Rev. Phys. Chem.* **2007**, *58*, 635–673.
51. Sewall, S. L.; Cooney, R. R.; Dias, E. A.; Tyagi, P.; Kambhampati, P. State-Resolved Observation in Real Time of the Structural Dynamics of Multiexcitons in Semiconductor Nanocrystals. *Phys. Rev. B* **2011**, *84*, 235304.
52. Sagar, D.; Cooney, R.; Sewall, S.; Dias, E.; Barsan, M.; Butler, I.; Kambhampati, P. Size Dependent, State-Resolved Studies of Exciton-Phonon Couplings in Strongly Confined Semiconductor Quantum Dots. *Phys. Rev. B* **2008**, *77*, 235321.
53. Saari, J. I.; Dias, E. A.; Reifsnyder, D.; Krause, M. M.; Walsh, B. R.; Murray, C. B.; Kambhampati, P. Ultrafast Electron Trapping at the Surface of Semiconductor Nanocrystals: Excitonic and Biexcitonic Processes. *J. Phys. Chem. B* **2013**, *117*, 4412–4421.
54. Klimov, V. I.; Mikhailovsky, A. A.; Xu, S.; Malko, A.; Hollingsworth, J. A.; Leatherdale, C. A.; Eisler, H.-J.; Bawendi, M. G. Optical Gain and Stimulated Emission in Nanocrystal Quantum Dots. *Science* **2000**, *290*, 314–317.
55. Guyot-Sionnest, P.; Wehrenberg, B.; Yu, D. Intraband Relaxation in CdSe Nanocrystals and the Strong Influence of the Surface Ligands. *J. Chem. Phys.* **2005**, *123*, 074709.
56. Cooney, R.; Sewall, S.; Dias, E.; Sagar, D.; Anderson, K.; Kambhampati, P. Unified Picture of Electron and Hole

Relaxation Pathways in Semiconductor Quantum Dots. *Phys. Rev. B* **2007**, *75*, 245311.
57. Klimov, V. Optical Nonlinearities and Ultrafast Carrier Dynamics in Semiconductor Nanocrystals. *J. Phys. Chem. B* **2000**, *104*, 6112–6123.
58. Califano, M.; Franceschetti, A.; Zunger, A. Lifetime and Polarization of the Radiative Decay of Excitons, Biexcitons, and Trions in CdSe Nanocrystal Quantum Dots. *Phys. Rev. B* **2007**, *75*, 115401.
59. Fernée, M. J.; Sinito, C.; Louyer, Y.; Potzner, C.; Nguyen, T.-L.; Mulvaney, P.; Tamarat, P.; Lounis, B. Magneto-Optical Properties of Trions in Non-Blinking Charged Nanocrystals Reveal an Acoustic Phonon Bottleneck. *Nat. Commun.* **2012**, *3*, 1287.
60. Nirmal, M.; Norris, D.; Kuno, M.; Bawendi, M.; Efros, A.; Rosen, M. Observation of the "Dark Exciton" in CdSe Quantum Dots. *Phys. Rev. Lett.* **1995**, *75*, 3728–3731.
61. Sewall, S. L.; Cooney, R. R.; Kambhampati, P. Experimental Tests of Effective Mass and Atomistic Approaches to Quantum Dot Electronic Structure: Ordering of Electronic States. *Appl. Phys. Lett.* **2009**, *94*, 243116.
62. Efros, A. L.; Rosen, M.; Kuno, M.; Nirmal, M.; Norris, D. J.; Bawendi, M. Band-Edge Exciton in Quantum Dots of Semiconductors with a Degenerate Valence Band: Dark and Bright Exciton States. *Phys. Rev. B* **1996**, *54*, 4843–4856.
63. Korkusinski, M.; Voznyy, O.; Hawrylak, P. Fine Structure and Size Dependence of Exciton and Biexciton Optical Spectra in CdSe Nanocrystals. *Phys. Rev. B* **2010**, *82*, 245304.
64. García-Santamaría, F.; Brovelli, S.; Viswanatha, R.; Hollingsworth, J.; Htoon, H.; Crooker, S.; Klimov, V. Breakdown of Volume Scaling in Auger Recombination in CdSe/CdS Heteronanocrystals: The Role of the Core–Shell Interface. *Nano Lett.* **2011**, *11*, 687–693.
65. Keene, J. D.; McBride, J. R.; Orfield, N. J.; Rosenthal, S. J. Elimination of Hole-Surface Overlap in Graded CdS_xSe_{1-x} Nanocrystals Revealed by Ultrafast Fluorescence Upconversion Spectroscopy. *ACS Nano* **2014**, *8*, 10665–10673.
66. Gao, Y.; Sandeep, C. S. S.; Schins, J. M.; Houtepen, A. J.; Siebbeles, L. D. A. Disorder Strongly Enhances Auger Recombination in Conductive Quantum-Dot Solids. *Nat. Commun.* **2013**, *4*, 3329.
67. Qu, L.; Peng, X. Control of Photoluminescence Properties of CdSe Nanocrystals in Growth. *J. Am. Chem. Soc.* **2002**, *124*, 2049–2055.
68. Cho, C.-H.; Aspetti, C. O.; Turk, M. E.; Kikkawa, J. M.; Nam, S.-W.; Agarwal, R. Tailoring Hot-Exciton Emission and Lifetimes in Semiconducting Nanowires *via* Whispering-Gallery Nanocavity Plasmons. *Nat. Mater.* **2011**, *10*, 669–675.
69. Exarhos, A. L.; Turk, M. E.; Kikkawa, J. M. Ultrafast Spectral Migration of Photoluminescence in Graphene Oxide. *Nano Lett.* **2013**, *13*, 344–349.
70. Takeda, J.; Nakajima, K.; Kurita, S.; Tomimoto, S.; Saito, S.; Suemoto, T. Time-Resolved Luminescence Spectroscopy by the Optical Kerr-Gate Method Applicable to Ultrafast Relaxation Processes. *Phys. Rev. B* **2000**, *62*, 10083–10087.
71. Arzhantsev, S.; Maroncelli, M. Design and Characterization of a Femtosecond Fluorescence Spectrometer Based on Optical Kerr Gating. *Appl. Spectrosc.* **2005**, *59*, 206–220.
72. Jasieniak, J.; Smith, L.; Van Embden, J.; Mulvaney, P.; Califano, M. Re-Examination of the Size-Dependent Absorption Properties of CdSe Quantum Dots. *J. Phys. Chem. C* **2009**, *113*, 19468–19474.